and, from (11) and (12),

$$f^2=1-\frac{(\lambda/\kappa r_1)^2 h_e^2}{[\cosh(fd/\lambda)+\frac{1}{2}s\alpha\sinh(fd/\lambda)]^2}\{\tfrac{1}{2}[(\lambda/2df)\sinh(2df/\lambda)+1]$$
$$+(d/d_1\gamma^2f^2)[(\lambda/2df)\sinh(2df/\lambda)-1]+(1/\gamma^2f^2)[\cosh(2df/\lambda)-1]\}. \quad \text{(A11)}$$

The average value of A is found to be

$$\langle A\rangle_{\rm av}=\frac{\phi_0}{2\pi r_1^2}h_e r_1\frac{(\lambda/fd)\sinh(fd/\lambda)+(2/\gamma^2f^2)[\cosh(fd/\lambda)-1]}{\cosh(fd/\lambda)+\frac{1}{2}s\alpha\sinh(fd/\lambda)}. \quad \text{(A12)}$$

Here we have used the abbreviations

$$\phi_0=hc/2e, \quad \text{(A13)}$$

$$h_e=2\pi r_1 d_1 H_e/\phi_0. \quad \text{(A14)}$$

PHYSICAL REVIEW VOLUME 181, NUMBER 2 10 MAY 1969

Flux Creep in Type-II Superconductors

M. R. BEASLEY,* R. LABUSCH,† AND W. W. WEBB
Department of Applied Physics and Laboratory for Atomic and Solid State Physics, Cornell University, Ithaca, New York 14850

(Received 3 January 1969)

We have made measurements of the evanescent decay of the irreversible magnetization induced by magnetic cycling of solid superconducting cylinders in order to elucidate the mechanisms of Anderson's thermally activated flux-creep process. A superconducting quantum interferometer device coupled to the creep specimen by a superconducting flux transformer made possible observations of flux changes with a resolution of one part in 10^9. The general applicability of Anderson's theory of flux creep was confirmed and the results were analyzed to show that: (1) The total flux in the specimen changed logarithmically in time, i.e., $\Delta\phi\propto\ln t/t_0$. (2) The logarithmic creep rate $d\phi/d\ln t$ is proportional to the critical current density J_c and to the cube of the specimen radius. (3) The logarithmic creep rate appears to be only weakly temperature-dependent because a proportionality to T is nearly compensated by the proportionality to J_c, which decreases as T increases. (4) The creep process is a bulk process that is not surface-limited (in this case). (5) Flux enters and leaves the surface in discrete events containing from about one flux quantum up to at least 10^3 flux quanta. (6) On departing from the critical state to a subcritical condition, the creep process tends to remain logarithmic in time, but the rate is decreased exponentially by decreasing T and is decreased extremely rapidly by backing off of the applied field from the critical state. (7) At magnetic fields $H<H_{c1}$ on the initial magnetization curve, no flux creep was observed, but the logarithmic creep rate showed a modest increase above H_{c1} and a broad rise as H approached H_{c2}. The creep process is characterized by a dimension parameter VX consisting of a flux bundle volume V and pinning length X, and by an energy U_0, both of which are supposed to be material-sensitive parameters characteristic of the irreversible processes. These parameters were determined from the experiments. Bundle volumes $V\approx10^{-12}$ cm^3 and energies $U_0\approx1$ eV were found, indicating that groups of fluxoids must be pinned and must move cooperatively. The results are found compatible with a recent model for flux pinning that includes these cooperative effects.

I. INTRODUCTION

BASIC to our present understanding of the remarkable current-carrying capacity and characteristic magnetic hysteresis of hard superconductors are the critical-state model[1,2] and Anderson's[3] theory of flux creep. In the critical-state model the virtually static hysteretic internal field and current distributions are ascribed to the pinning of the fluxoid distribution against the electromagnetic driving forces by material inhomogenieties. The Anderson-Kim[3,4] theory of flux creep describes *dynamic* effects arising from the thermally activated motion of the fluxoids past the pinning barriers and thus generalizes the concept of the critical

* Now at Division of Engineering and Applied Physics, Harvard University, Cambridge, Mass.
† Now at the Institut für Metallphysik, Göttingen, Germany.
[1] C. P. Bean, Phys. Rev. Letters 8, 250 (1962).
[2] Y. B. Kim, C. F. Hempstead, and A. R. Strnad, Phys. Rev. 129, 528 (1963).
[3] P. W. Anderson, Phys. Rev. Letters 9, 309 (1962).
[4] P. W. Anderson and Y. B. Kim, Rev. Mod. Phys. 36, 39 (1964).

state. In particular, it defines the sense in which there is a well-defined critical current and predicts a slowly decreasing decay rate for the persistent currents in hard superconductors.

The critical-state model appears to provide a satisfactory description of the transport current and magnetization measurements on hard superconductors, except at low fields in very-low-κ materials, where surface effects are believed to be important.[5] In addition, many qualitative and some quantitative studies of the critical current density in the critical state have been made in a search for better understanding of pinning mechanisms.[6]

However, the only substantial experimental studies of the flux-creep process are the original studies of Kim, Hempstead, and Strnad.[7,8] They observed the logarithmic decay of the persistent current due to flux creep in hollow cylinders of hard superconductors and convincingly demonstrated the basic ideas of Anderson's theory in studies of the resistive transitions at the critical transport current in hard superconductors. In neither of these original studies was the flux-creep process systematically studied over a range of conditions. We suppose that it is the difficulty of the necessary measurements of very small changes of magnetization that has inhibited the characterization of the flux-creep process.

This paper reports an experimental investigation and theoretical analysis of the flux-creep process. We have aimed to improve our basic understanding of the flux-creep process and to use flux-creep measurements as a means of studying the basic pinning mechanisms operative in hard superconductors. We have observed flux creep in some typical hard superconductors by measuring changes in the average magnetization as the nonequilibrium currents in the material decayed via flux creep, and have compared the results with the behavior expected on the basis of the Anderson-Kim theory. We studied a series of plastically deformed lead alloys in the critical state, along the initial magnetization curve, at fields above H_{c2}, and after departures from the critical state effected by changing field or temperature. The effects of cold working, specimen size, and temperature were investigated for magnetic histories in the critical state.

This paper is divided into several major parts. In Sec. II the Anderson-Kim theory of flux creep is outlined, the equations are solved for the rate of flux transport through the surfaces of solid cylinders such as were used in these experiments, and the solution reformulated to facilitate display of the relationships between the material-sensitive parameters and the characteristic quantities describing the flux-creep process. The experimental techniques are outlined in Sec. III, where we briefly describe the highly sensitive magnetometer (based on quantum interference effects in superconductors) that was specially developed for these experiments. In Sec. IV the results are presented and in Sec. V they are compared with theory and analyzed to identify the characteristics of the flux-creep process. For one alloy, the material-sensitive parameters were determined as a function of magnetic induction and amount of cold working. In Sec. VI the results are compared with current models of fluxoid pinning, and are found fully compatible with a pinning model proposed by Labusch[9] and Fietz and Webb,[6] in which cooperative interactions between pinning points lead naturally to the large activation energies and flux bundle volumes observed in the flux-creep experiments.

II. THEORETICAL ANALYSIS OF FLUX CREEP

A. Flux-Creep Equation

According to the critical-state model, at $T=0$ the fluxoids in the bulk of a hard superconductor can move only if the driving-force density F acting on them exceeds the maximum local pinning-force density F_p. In magnetization experiments, the driving force arises from a density gradient in the distribution of mutually interacting fluxoids and, as shown by Friedel, DeGennes, and Matricon,[10] is given by the Lorentz-like relation[11]

$$\mathbf{F}=-\frac{1}{c}\mathbf{J}\times\mathbf{B}\frac{\partial H(B)}{\partial B}=-\frac{\gamma}{4\pi}\mathbf{B}\times(\nabla\times\mathbf{B}), \quad (2.1a)$$

which assumes the useful "one-dimensional" scalar forms

$$F=\gamma BJ/c=-\gamma B\nabla B/4\pi, \quad (2.1b)$$

where $H(B)$ is the magnetic field that would be in thermodynamic equilibrium with the magnetic induction B inside the superconductor, and $\gamma\equiv\partial H(B)/\partial B$. J is the current density corresponding to the macroscopic flux density gradients.

When a sufficiently large magnetic field is applied to a hard superconductor, an internal gradient in the flux density is formed beginning at the surface, and fluxoids eventually force their way past the pinning barriers into the material. Inside the material, the fluxoids relax into an arrangement such that F just equals F_p everywhere. When this balance of forces is reached, the material is said to be in the critical state, and the circulating persistent currents are uniquely determined if $F_p(B)$ is known.

[5] For a review of these studies with a list of references, see J. D. Livingston and B. W. Schadler, Progr. Mater. Sci. **12**, 183 (1964).

[6] See W. A. Fietz and W. W. Webb, Phys. Rev. **178**, 657 (1969).

[7] Y. B. Kim, C. F. Hempstead, and A. R. Strnad, Phys. Rev. Letters **9**, 306 (1962).

[8] Y. B. Kim, C. F. Hempstead, and A. R. Strnad, Phys. Rev. **131**, 2486 (1963).

[9] R. Labusch (unpublished).

[10] J. Fridel, P.-G. DeGennes, and J. Matricon, Appl. Phys. Letters **2**, 119 (1963).

[11] In this expression and throughout this paper, the symbol B signifies the magnitude of the field in the z direction and is not a vector quantity unless explicitly shown in bold type (e.g., **B**). Also, all vector operators operate only in the xy plane.

However, as first pointed out by Anderson,[3] at nonzero temperature, fluxoid motion (or flux creep) is possible with the help of thermal activation even if $F<F_p$. Thus, after an applied field change, fluxoids continue to move, relaxing the driving force, even as F approaches and falls below F_p. The rate of thermally activated motion is strongly enhanced by the driving force F, and as F falls below F_p, the rate of fluxoid motion decreases extremely rapidly. When this rate becomes small enough to be negligible in a conventional magnetization measurement, the superconductor is again said to be in the critical state. Therefore, the critical state exists for $T>0$ only as a somewhat indistinct condition, but it turns out that the amount of flux motion involved in flux creep over any reasonable time scale is so small that F still essentially equals F_p, and the uncertainty in the critical state is quite small. Of course, the "persistent" currents associated with the flux gradients in the critical state will continuously decay, even if very slowly, and it is just these decays which were studied in this investigation. We now proceed to an analysis of the characteristics of these decays based on Anderson's theory of flux creep.

According to the Anderson theory of flux creep, the rate at which "flux bundles" jump over the pinning barriers is given by the usual Arrhenius expression

$$\nu=\nu_0 e^{-U/kT}, \tag{2.2}$$

where ν_0 is an attempt frequency and U is an effective activation energy. The term "flux bundle" describes the cluster of neighboring fluxoids, coupled by their mutual interactions, that is supposed to act collectively in each thermally activated event. Thermally activated motion will be strongly assisted by the driving force $\mathbf{F}$, and therefore U should be a decreasing function of $|\nabla B|$, and for all practical purposes the fluxoids should move only down the field gradient. To account for the fact that U is a decreasing function of $|\mathbf{F}|$, Anderson and Kim used the linear relation

$$U=U_0-|\mathbf{F}|VX, \tag{2.3}$$

which is the simplest functional form with the correct physical features. In this relation, U_0 was presumed to be the effective height of the energy barrier for thermally activated motion of a flux bundle and the term $|\mathbf{F}|VX$ represents the decrease in the height of the barrier due to applied forces. V is the activation (or flux bundle) volume. We call X the pinning length; it is the effective geometrical width of the energy barrier. Nonlinearities in U as a function of $|\nabla B|$ require a more careful interpretation of U_0 and X to be given later, but the above picture is essentially correct and will suffice for now. One of our objectives is to deduce from flux-creep experiments the values of U_0, V, and X.

In order to analyze flux-creep experiments, it is necessary to develop solutions for the flux-transport problem in macroscopic specimen geometries, a problem analogous to solving a nonlinear diffusion equation for mass transport, where the diffusion constant is a strong function of the potential gradient. We proceed here with this problem.

The flux-flow density $\mathbf{D}$, i.e., the amount of flux that crosses a line perpendicular to B and ∇B per unit length and time, is conveniently written

$$\mathbf{D}=-(\nabla B/|\nabla B|)Bw\nu_0 e^{-U(B,|\nabla B|)/kT}, \tag{2.4}$$

where w is the average distance by which a flux bundle moves in a thermally activated jump, and where in writing $U=U(B,|\nabla B|)$ we have taken B as always positive but ∇B may have either sign. Since no detailed theory of the depinning process is available, we assume that w is some unknown function of B and ∇B. However, it turns out that the results of the analysis for the rate of flux creep are virtually independent of w and ν_0, so that the actual values and functional form of these quantities are unimportant. Conservation of flux requires $\partial B/\partial t=-\nabla\cdot\mathbf{D}$ and gives the flux-creep equation

$$\partial B/\partial t=\nabla\cdot[(\nabla B/|\nabla B|)Bw\nu_0 e^{-U(B,|\nabla B|)/kT}]. \tag{2.5}$$

Using Eq. (2.3) for U, Anderson and Kim solved the flux-creep equation for the geometry of a thin hollow cylinder. The calculated result is a logarithmic decay in time of the persistent current circulating around the cylinder in the critical state. This logarithmic decay was observed experimentally by Kim, Hempstead, and Strnad who, as we mentioned before, also studied flux flow in a steady-state situation, where the flux-flow rate was held constant with an applied transport current. These experiments have demonstrated the exponential dependence of the flux-flow rate on U/kT and the linear dependence of U on F, in the limited field range of the reported experiments.

The solution of Eq. (2.5) required for a thin hollow cylinder is simplified by the assumption that the flux-flow density $\mathbf{D}$ is constant throughout the specimen and therefore only a function of time. Unfortunately, this assumption is certainly not valid in the more general case of a thick sample, and a better solution is required. The experiments reported in this paper were performed on solid cylinders, and thus we shall restrict our calculations to cylindrical symmetry but will not assume $\mathbf{D}$ independent of r. In this case, Eq. (2.5) becomes

$$\frac{\partial B}{\partial t}=-\frac{1}{r}\frac{\partial}{\partial r}(rD), \tag{2.6}$$

where D is the radial component of $\mathbf{D}$.

It turns out to be convenient to calculate the flux-flow density D rather than B. Once D is known as a function of r and t (D is an explicit function of B and ∇B, and is therefore an implicit function of r and t), $\partial B/\partial t$ can be obtained from Eq. (2.6). The total flux which enters or leaves the specimen, the experimentally

observable quantity, is simply obtained from the relation

$$\partial\phi/\partial t = -2\pi\rho D(\rho,t),$$

where ϕ is the total flux in the specimen and ρ is the specimen radius. Since

$$\frac{\partial D}{\partial t}=\frac{\partial D}{\partial B}\frac{\partial B}{\partial t}\pm\frac{\partial D}{\partial|\nabla B|}\frac{\partial(\nabla B)}{\partial t},$$

we obtain, using Eqs. (2.5) and (2.6),

$$\frac{\partial D}{\partial t}=\frac{\partial D}{\partial B}\frac{1}{r}\frac{\partial(rD)}{\partial r}\pm\frac{\partial D}{\partial|\nabla B|}\frac{\partial}{\partial r}\left(\frac{1}{r}\frac{\partial(rD)}{\partial r}\right), \quad (2.7a)$$

where

$$\frac{\partial D}{\partial B}=\frac{D}{kT}\left[\frac{\partial U}{\partial B}-kT\frac{\partial(\ln Bw\nu_0)}{\partial B}\right] \quad (2.7b)$$

and

$$\frac{\partial D}{\partial|\nabla B|}=\frac{D}{kT}\left[\frac{\partial U}{\partial|\nabla B|}-kT\frac{\partial(\ln Bw\nu_0)}{\partial|\nabla B|}\right]. \quad (2.7c)$$

The $\pm$ signs refer to positive and negative $\nabla B=\partial B/\partial r$, respectively.

B. Solution to Flux-Creep Equation in the Critical State

Equation (2.7) can be solved fairly simply when the sample is in the critical state, where we expect the condition $U\gg kT$ to hold. The solution obtained is the lowest-order solution in an expansion in powers of kT/U, and will be sufficiently accurate for our purposes. In this section we obtain the first-order solution. It can be shown that the corrections to this solution are of higher order in kT/U.

From the definition of **D**, Eq. (2.4), we obtain the relation that $\delta(kT\ln Bw\nu_0-U)=kT\delta(\ln D)=kT\delta D/D$, where δ represents changes with respect to either time or space. From this relation we can deduce two useful simplifications of Eqs. (2.7). First, we see that relative changes of $U-kT\ln Bw\nu_0$ in time are roughly a factor of kT/U smaller than relative changes in D and therefore negligible compared to changes in D itself. Thus, in calculating $\partial D/\partial B$ and $\partial D/\partial|\nabla B|$, we can neglect the time dependence of the quantities in the brackets of Eqs. (2.7b) and (2.7c) compared to that of D and evaluate them at some time t_1 after the critical state is established. Since the time dependence of all these quantities is extremely small, the exact value of t_1 is not important, and any value of the quantity representative of the critical state is acceptable. Second, we find that, since D is not expected to vary rapidly in either space or time,[12] $\delta(\ln D)$ is of order unity, and therefore relative changes in $U-kT(\ln)Bw\nu_0$ are of order $kT/U\ll 1$. Thus, to a good approximation the total derivative of $U-kT\ln Bw\nu_0$ with respect to r is equal to zero. This leads to the relation

$$\frac{\partial(U-kT\ln Bw\nu_0)}{\partial B}=\pm\frac{\partial\ln|\nabla B|}{\partial r}\frac{\partial(U-kT\ln Bw\nu_0)}{\partial|\nabla B|},$$

which relates the two partial derivatives needed to evaluate $\partial D/\partial B$ and $\partial D/\partial|\nabla B|$. Again, the $\pm$ signs refer to positive and negative $\nabla B=\partial B/\partial r$, respectively. Substituting this last relation into the flux-creep equation and keeping only the time dependence of D, we find

$$\frac{\partial D}{\partial t}=\pm\frac{D}{kT}\left(\frac{\partial U}{\partial|\nabla B|}\right)_{t_1}\left[\frac{\partial}{\partial r}\left(\frac{1}{r}\frac{\partial(rD)}{\partial r}\right)-\frac{\partial(rD)}{r\partial r}\left(\frac{\partial\ln|\nabla B|}{\partial r}\right)_{t_1}\right], \quad (2.8)$$

where the subscript t_1 indicates that the quantities are to be evaluated at time t_1 and are functions of r only, and where in this last step we have made the additional minor approximation that there is no strong dependence of $\ln Bw\nu_0$ on ∇B and therefore $\partial(U-kT\ln Bw\nu_0)/\partial|\nabla B|\approx\partial U/\partial|\nabla B|$.

A particular integral of the differential equation is easily found: With $D(r,t)=\Delta(t)\psi(r)$, the equation is separated into a purely time-dependent part

$$\frac{\partial\Delta}{\partial t}=\pm\Delta^2(t), \quad (2.9a)$$

and a purely position-dependent part

$$\frac{1}{kT}\left(\frac{\partial U}{\partial|\nabla B|}\right)_{t_1}\left[\frac{\partial}{\partial r}\left(\frac{1}{r}\frac{\partial(r\psi)}{\partial r}\right)-\left(\frac{\partial\ln|\nabla B|}{\partial r}\right)_{t_1}\left(\frac{1}{r}\frac{\partial(r\psi)}{\partial r}\right)\right]=1. \quad (2.9b)$$

The solution of Eq. (2.9a) is

$$\Delta(t)=\mp 1/t. \quad (2.10)$$

(The integration constant can be eliminated by an appropriate choice of the time zero.)

The general solution of Eq. (2.9b) is

$$-r\psi=kT\int_{r_1}^{r}X|\nabla B|_{t_1}\times\left[\int_X^{r_2}\frac{dX'}{(\partial U/\partial|\nabla B|)_{t_1}|\nabla B|_{t_1}}\right]dX, \quad (2.11)$$

which is easily verified by inserting $r\psi$ into Eq. (2.9b).

[12] Our solution to the creep equation will show that $D\sim 1/t$ and has the fastest spatial variation near the origin, where $D\propto 1/r$. Therefore, $\delta\ln D$ is of order unity for any reasonable time scale, except for a very small region near the origin which is not physically significant, being on a scale finer than the dimension of a fluxoid.

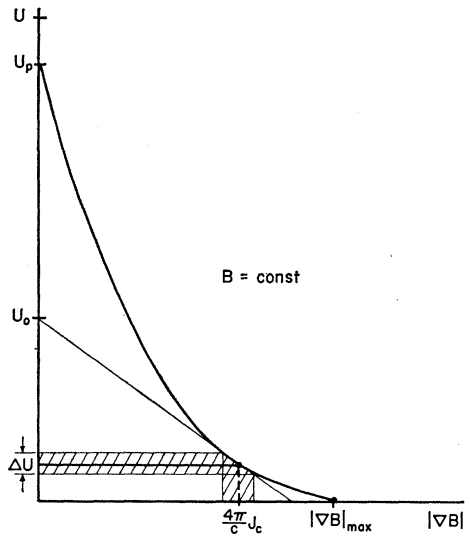

FIG. 1. Typical dependence of the activation energy U on the field gradient $|\nabla B|$ at fixed B. The curve illustrates the nonlinearities which arise if thermal activation is strongly assisted by the driving force, so that thermal activation depends on the top of the energy barrier. The shaded region represents the critical-state region. The tangent to the curve in the critical-state region intersects the ordinate at U_0, and its slope is $\gamma(B/4\pi)VX$. The effect of the nonlinearity of U on the connection between the parameters U_0 and X and the height U_p and width X_p of the actual energy barrier can be clarified by a model calculation. Consider a pinning potential of the form $U(X)=\frac{1}{2}U_p\cos(\pi X/X_p)$, where X is the position. The activation energy U is the difference between a minimum and the adjacent maximum of the function $\frac{1}{2}U_p\cos(\pi X/X_p)-fX$, where $f=\gamma(B/4\pi)|\nabla B|$, V is the total force acting on the barrier. The resultant function is actually illustrated here. When the force on the barrier is large and the thermal activation takes place near the top of the barrier, U is small compared to U_p and the function approaches the form $U=U_p(\frac{1}{3}\sqrt{8})\times(1-|\nabla B|/|\nabla B|_{max})^{3/2}$, where $|\nabla B|_{max}=4\pi^2U_p/X_pV\gamma B$ is the maximum field gradient which would be possible if there were no thermal activation (i.e., at $T=0$). Using this expression, it is simple to relate the observable quantities U_0 and X in terms of U_p, X_p, and U. With elementary algebra we obtain $U_0=U_p(\frac{3}{4})\times(4U_p)^{1/3}$ and $X=X_p(\frac{3}{2}\pi)(4U/U_p)^{1/3}$. Similar results would have been obtained with any smooth function instead of $\cos\pi\chi/X_p$ for the pinning potential.

The total flux in the specimen at the time t is given by

$$\phi(t)=\phi(t_0)\pm 2\pi\rho\psi(\rho)\ln(t/t_0), \qquad (2.12)$$

where ρ is the specimen radius and t_0 is an arbitrary reference time. From this last equation we find that the logarithmic derivative of the total flux in the specimen should be a constant, which we define as the logarithmic creep-rate constant

$$R\equiv d\phi/d\ln t=\pm 2\pi\rho\psi(\rho). \qquad (2.13)$$

More generally we could define a logarithmic creep rate as a function of position $R(r)=2\pi r\psi(r)$, but since it is the total flux change in the specimen which is measured experimentally, it is sufficient to consider only $R\equiv R(\rho)$.

To complete the solution it only remains to determine r_1 and r_2 in Eq. (2.11) from the boundary conditions and to evaluate the resulting expression for R. The boundary condition at the surface is determined if we assume that the flux flow through the surface is not obstructed by a surface barrier. Then the flux density at the surface has to be in equilibrium with the applied magnetic field, and therefore $\partial B/\partial t=0$ at the surface for a constant applied field. This requires $(\partial(rD)/\partial r)_{r=\rho}=0$ and therefore $r_2=\rho$ in Eq. (2.11). The second boundary condition, which is not actually needed for calculating R, is obtained from the requirement that $\partial B/\partial t$ be finite everywhere. In a solid cylinder this requires that $D(r)\propto r$ as r goes to zero and therefore $r_1=0$. Substituting Eq. (2.11) with the boundary conditions found above into the expression for R, we obtain the final result. This final result can be written in a closed form if we expand the functions $|\nabla B|_{t_1}$ and $(\partial U/\partial|\nabla B|)_{t_1}$ in the powers of $(\rho-r)$ around their values at the specimen surface. Keeping only first powers of $(\rho-r)$, we obtain

$$R=\pm\tfrac{1}{3}\pi kT\rho^3(\partial U/\partial|\nabla B|)_{t_1,\rho}^{-1}(1\pm\delta), \qquad (2.14a)$$

where

$$\delta=\tfrac{1}{4}\rho|\nabla B|_{t_1,\rho}\frac{\partial}{\partial B}\ln\left[\frac{1}{|\nabla B|_{t_1,\rho}}\left(\frac{\partial U}{\partial|\nabla B|}\right)_{t_1,\rho}\right]. \qquad (2.14b)$$

The $\pm$ signs refer to positive and negative $\nabla B=\partial B/\partial r$, corresponding to increasing and decreasing applied fields in the critical state. As indicated by the subscripts, all quantities are evaluated at the surface and at a fixed time t_1 in the critical state. The expansion used to obtain this last result is good if the correction factor δ is small compared to unity.

C. Discussion of the Theoretical Analysis

Our analysis shows that the characteristic logarithmic time dependence of the decays predicted by Anderson for hollow cylinders is preserved in the more general solution found here. In fact, in Appendix A, it is shown that any perturbation to the solution found in the last section produces nonlogarithmic transients that decay rapidly in time, so that for large t the creep rate always becomes logarithmic.

Equation (2.14a) indicates that the logarithmic creep rate R is proportional to ρ^3. This proportionality is characteristic of flux creep in the bulk. It arises because we have assumed that surface barriers are not controlling the rate of flux flow through the surface. If we assume that flux entry and exit are controlled by a surface barrier, we find that the logarithmic creep rate is proportional to ρ^2. Therefore, it is possible to differentiate experimentally between the two cases. A simple discussion of creep with a surface barrier is given in Appendix B.

Equation (2.14a) indicates that flux-creep measurements may yield the interesting quantity $(\partial U/\partial|\nabla B|)_{t_1}$. However, it is necessary to eliminate the correction factor $1\pm\delta$, even though it is close to unity. This factor takes into account the fact that in the integral solution

of the flux-creep equation [Eq. (2.11)], $|\nabla B|_{t_1}$ and $(\partial U/\partial|\nabla B|)_{t_1}$, being functions of B, differ as a function of position depending on whether the sample is in the critical state for increasing or decreasing applied fields. According to Eq. (2.14a), it is possible to eliminate the weighting corrections by using $R_{\rm av}=\frac{1}{2}(R\uparrow+R\downarrow)$, the average of the creep rates for increasing and decreasing applied fields, which should be independent of δ. This result suggests that the experimental data can be analyzed most simply using $R_{\rm av}$. In addition, the validity of the assumed expansion in powers of $(\rho-r)$ can be checked by computing δ from the relation

$$\frac{R\uparrow}{R\downarrow}=(1+\delta)/(1-\delta) \tag{2.15}$$

and confirming that $\delta<1$.

As we have already shown, the relative changes of the activation energy U with respect to time are expected to be of order $kT/U\ll 1$, and therefore the linear approximation $U=U_0-\gamma(B/4\pi)|\nabla B|VX$ made by Anderson and Kim is justified. However, we have not yet discussed the consequences of the fact that when the thermal activation takes place near the top of an energy barrier, U becomes a nonlinear function of $|\nabla B|$, and therefore the parameters U_0 and VX are not trivially related to the height U_p and width X_p of the actual energy barrier. The actual situation is illustrated schematically in Fig. 1. From the figure we see that $(\partial U/\partial|\nabla B|)_{t_1}$ and U_0 are the slope and intercept, respectively, of the tangent to the curve at some value of U lying in the relatively narrow shaded region representative of the critical state. We also see that if $U\ll U_0$, as we expect,

$$\left(\frac{\partial U}{\partial|\nabla B|}\right)_{t_1,\rho}=\frac{U_0}{4\pi J_c/c},$$

where J_c is the current density flowing at the surface in the critical state.

In terms of the parameters U_0 and VX, the expression in Eq. (2.14) for the logarithmic creep rate can be written

$$R=\frac{\pi}{3}kT\rho^3\frac{4\pi}{\gamma B}\frac{1}{VX}(1\pm\delta)=\frac{\pi}{3}kT\rho^3\frac{4\pi}{c}\frac{J_c}{U_0}(1\pm\delta), \tag{2.16a}$$

where

$$\delta=\frac{1}{2}\left(\frac{4\pi}{c}\right)\rho\left(\frac{1}{J_c}\frac{\partial \ln U_0}{\partial B}-\frac{\partial J_c}{\partial B}\right). \tag{2.16b}$$

To convert the equations to practical units (B in G, J in A/cm^2), it is sufficient to change $4\pi/c$ to $4\pi/10$. Equation (2.16) are our central result and indicate that flux-creep measurements, combined with critical-current measurements, allow determination of both material sensitive parameters of the theory, U_0 and VX. Conventional critical-current measurements alone only provide the ratio U_0/VX, and therefore flux-creep measurements provide essential additional information about the pinning mechanisms.

The model calculation discussed in Fig. 1 shows that the physical properties of the barrier are not given directly by the observable quantities but are closely related to them in a way that depends only weakly on its shape. Thus for all practical purposes Eq. (2.16) gives a satisfactory measure of the pinning energy U_p and the characteristic dimensional combination VX_p.

III. EXPERIMENTAL PROCEDURES

A. Magnetization-Change Measurements

The very slow magnetization changes associated with the flux-creep process were measured using a specially developed magnetometer incorporating a point-contact superconducting quantum interference device (SQUID) similar to that originally developed by Silver and Zimmerman.[13] The detailed design and operation of this special system have been reported elsewhere,[14] but since the use of quantum interference devices in actual experiments is relatively new and unfamiliar, we give a brief description of the system developed for these experiments. This system provides a practical scheme for using the extremely sensitive SQUID for measurements in high magnetic fields and should prove useful for a variety of magnetic measurements.

The experimental arrangement is shown in Fig. 2. Basically, the system operates as follows: A specimen is placed in a persistent-current high-field superconducting solenoid and coupled by means of a dc superconducting flux transformer to the SQUID. The SQUID is located in a carefully shielded region in order to isolate it from the large field changes of the solenoid. When the magnetization of the specimen in the flux-transformer primary changes, a persistent current develops in the transformer and reflects this magnetization change at the secondary, where its flux is detected by the SQUID, producing periodic modulation in the SQUID I-V (current-voltage) characteristic. Although the niobium point contact SQUID used in these experiments shows the characteristic modulation by flux even when placed directly in the high-field region, its detailed electrical characteristics are excessively dependent on the ambient field. For this reason, it is more convenient in practice to use the transformer-coupled arrangement to keep the SQUID in a region of constant field and thereby stabilize its electrical characteristics.

It was also found that the electrical characteristics of the SQUID were very sensitive to stray electromagnetic

[13] A. H. Silver and J. E. Zimmerman, Phys. Rev. **141**, 367 (1966).

[14] M. R. Beasley, Ph.D. thesis, Cornell University, 1968 (unpublished); M. R. Beasley and W. W. Webb, in *Proceedings of the Virginia Conference on the Physics of Superconducting Devices* (University of Virginia, Charlottesville, 1967), p. V-1.

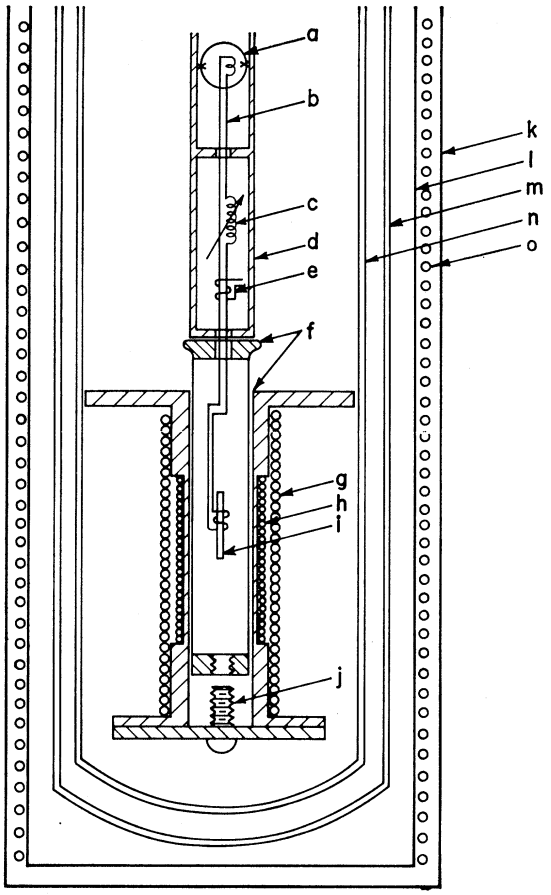

FIG. 2. Schematic of complete magnetometer system. (a) SQUID surrounding superconducting-transformer secondary; (b) superconducting dc transformer; (c) additional inductance in superconducting-transformer circuit to change transfer ratio between primary and secondary; (d) superconducting Pb shield; (e) thermal switch to open transformer circuit during large field changes; (f) shoulder to seat magnetometer support assembly firmly in top plate of magnet in order to reduce microphonics due to the motion of the transformer primary in the high field; (g) 2500-G persistent-current superconducting Nb solenoid; (h) copper solenoid to make small field changes while superconducting magnet is in persistent current mode; (i) magnetic specimen in superconducting transformer primary; (j) tapped hole and stud to secure magnetometer assembly firmly to bottom plate while seating shoulder (f); (k) and (l) Mumetal magnetic shielding; (m) liquid-nitrogen Dewar; (n) helium Dewar; (o) coil to demagnetize Mumetal shields.

radiation. Therefore, to provide adequate electromagnetic shielding the entire experiment was placed in an rf-shielded enclosure and the Dewars mounted inside two concentric Mumetal cans. The Mumetal cans also shielded the SQUID against fluctuations in the local magnetic field. When shielded in this manner, the transformer-coupled SQUID provided reliable operation with stable electrical characteristics over an entire day's operation and achieved a field sensitivity of 10^{-7} G in a field of 2000 G for a field resolution of 1 part in 10^{10}.

One remaining difficulty in the operation of this system was small drifts in the magnetometer output due to flux creep in the material comprising the superconducting transformer. These drifts are not unique to the transformer-coupled arrangement, and were also present when the SQUID was placed directly in the high magnetic field and flux entered the material comprising the SQUID. In practice, the drifts seemed more manageable with the transformer, and were not a serious problem in these experiments.

The periodic modulation of the SQUID I-V characteristic arising from flux changes in the specimen was detected using the ac field-modulation scheme shown in Fig. 3. A dc current biases the SQUID on the sensitive part of its I-V characteristic where the modulation is largest, and an ac modulating field is applied to the SQUID. The output signal of the SQUID is periodic with period $\phi_0 = 2.1\times10^{-7}$ G cm^2 in the total flux (both ac and dc) that passes through the nonsuperconducting area enclosed by the SQUID, but after phase-sensitive detection at the modulating frequency, the resultant signal is periodic only in the dc flux changes. (The signals at the various points in the detection circuit are shown in Fig. 3.) With the transformer-coupled arrangement the dc flux changes seen by the SQUID are produced by the transformer secondary, and therefore the output voltage of the system is effectively of the form $V = V_0 \cos 2\pi\alpha\phi/\phi_0$, where α is the flux gain of the transformer and ϕ is the total flux in the specimen.

For the flux-creep measurements reported here, the transformer was designed to make $\alpha \approx 0.01$ in order to ensure that the largest abrupt flux changes that occurred in the creep process did not produce more than half a cycle in the output signal. This arrangement sacrificed sensitivity, but it eliminated any ambiguity in the actual amount of flux change, and as flux slowly entered or left the specimen the output signal was a series of discontinuous steps forming a sinusoid with a period depending on the average rate of flux change. Figure 4 shows a tracing of a typical magnetometer output signal during a flux-creep measurement.

The actual measuring procedure consisted of setting a dc field with the persistent-current superconducting solenoid, ramping a small copper coil located inside the solenoid to the final field, and then observing the subsequent flux creep with the mangetometer. The small

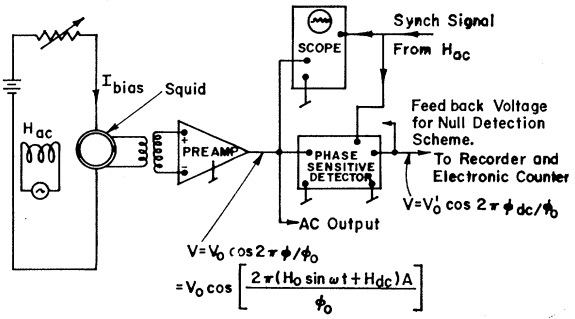

FIG. 3. SQUID detection circuit.

ramping field was necessary in order to ensure that the approach to the final field was monotonic (small departures in the opposite direction drastically affect the rate of flux creep) and to provide a well-defined zero of time. Normally a ramp of 50 G in 1 sec was used, and it was established experimentally that the exact ramp rate did not affect the observed creep rate. The copper ramping coil was designed to minimize coupling with the persistent-current magnet and thus minimize its cancellation.

The sinusoidal magnetometer output signal was processed by electronically counting the number of complete cycles and plotting the total number versus ln$t$ (the expected time dependence) on an X-Y recorder. Figure 5 shows a series of typical recordings for various magnetic histories. Since each complete cycle in the magnetometer output corresponds to a change of approximately 100 ϕ_0 in the average flux passing through the specimen, the curves are in effect a plot of average magnetization change versus ln$t$. The vertical steps in these recorder tracings reflect the incremental nature of the counting process and are *not* related to the abrupt changes in the flux through the specimen seen in Fig. 4. The steps in Fig. 5 are produced by the event counter, which simply provides a voltage increment at the time that a specified number of counts have been detected. The physically significant steps shown in Fig. 4 will be discussed later.

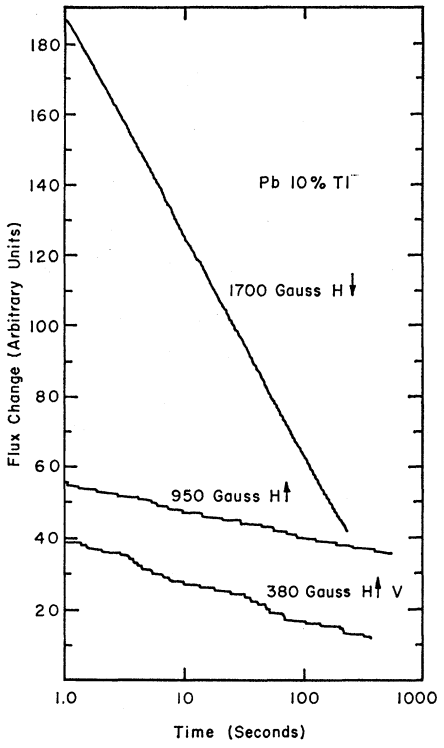

FIG. 5. X-Y recording of flux change versus ln t. Typical behavior at high and low fields for creep on the initial magnetization curve (indicated by V). In this record the vertical steps are due only to the digital nature of the signal processing (each step indicates the completion of a full cycle in the magnetometer output) and are not due to discontinuous flux changes in the sample. The arrows indicate whether H was increasing or decreasing.

B. Specimen Preparation

Cylindrical rods of several PbTl alloys containing 0.6%, 4.5%, and 10% Tl were prepared by careful melting procedures under the supervision of Professor J. L. Gregg in the Materials Science Center Metallurgical Facility at Cornell University. Cylindrical wire specimens for flux-creep measurements were prepared by extrusion of these rods at liquid-nitrogen temperature from an initial diameter of about 0.75 cm to final diameters of 0.086–0.190 cm (that is, about 34–75 mil). The extruded wires were stored in liquid nitrogen to prevent annealing and change of surface condition subsequent to extrusion.

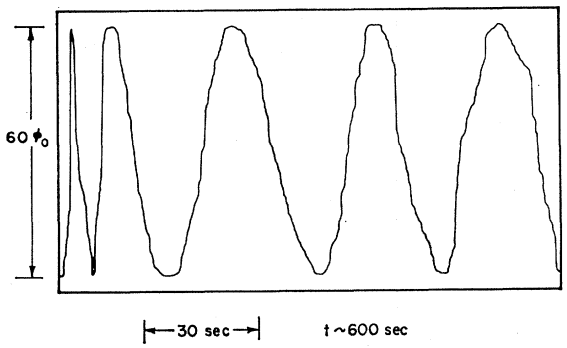

FIG. 4. SQUID detector output during flux creep. This tracing of a typical strip chart recording illustrates the discrete nature of the flux changes during the flux-creep process. The size of the steps shown indicates the amount of flux in each event that couples with the superconducting transformer and represents a lower limit to the actual amount of flux change in a particular event.

It is expected that the severe plastic deformation produced by single-stage extrusion with a factor-of-10 reduction of area would produce macroscopically homogeneous dislocation concentrations. To obtain various less-severe levels of deformation, that is, lower dislocation concentrations, some of the extruded specimens were annealed for several minutes at room temperature. It was found that the critical current densities J_c could be reduced by about a factor of five by a 2-min room-temperature anneal.

The specimen wires were sufficiently long to neglect demagnetization-factor effects, having always lengths of several centimeters, which is many times the wire diameter and many times either the diameter or the length of the pickup coils.

The critical current densities of the specimens studied were deduced from measurements of the hysteretic magnetization curves, using essentially the procedure of Fietz, Beasley, Silcox, and Webb.[15] The values of $J_c(H)$

[15] W. A. Fietz, M. R. Beasley, J. Silcox, and W. W. Webb, Phys. Rev. **136**, A335 (1964).

remained unchanged by long periods of storage at liquid-nitrogen temperature and may be regarded as characteristic of the individual specimens. These data are given later.

Creep experiments were also carried out on some PbIn alloys purchased in wire form from the United Mineral and Chemical Corporation. However, the results were similar, and are not discussed in this paper because the conclusions appear redundant and the data recorded on that series of alloys were taken as an exploratory venture.

IV. RESULTS

Our main results can be cataloged on the basis of the features of Eqs. (2.16) for the logarithmic creep rate $R=d\phi/d\ \ln t$. First, our measurements of the time dependence of the total flux subsequent to magnetic cycling into the critical state are considered, in order to establish whether creep in the critical state really is characterized by a logarithmic creep-rate constant R. On finding that logarithmic creep really is observed, the dependence of the logarithmic creep-rate constant R on the relevant experimental parameters, magnetic field H, critical current J_c, specimen radius ρ, and temperature T, is considered. Next the effects on the creep rate of excursions in T or H away from the critical state are reported, and finally some direct observations on the "sizes" of the increments of flux crossing the specimen surface are given. The problem of deducing the material-sensitive parameters U_0, VX, and δ is deferred to Sec. V.

As expected the total magnetic flux in the specimens in the critical state or on the initial magnetization curve was observed to decay logarithmically in time. Examples of these decays are shown in Fig. 5 where in each case the long-term behavior is clearly proportional to the logarithm of time. The decays at high fields were always smooth and reproducible logarithmic functions of time. Only for the lowest-field curve are there any significant short-term derivations from the over-all logarithmic behavior. Somewhat erratic behavior seems to be characteristic of the low-applied-field region where the decays were frequently observed to be a little irregular and sometimes irreproducible.

Because the decays always were logarithmic in time, we need only specify the logarithmic creep rate $R=d\phi/d\ \ln t$ in order to describe the experimental data on flux-creep behavior under any given condition. The small drifts in the magnetometer due to flux creep in the superconducting transformer winding also showed the logarithmic time dependence and were quite reproducible for a given magnetic history. Thus, it was possible to correct for these drifts by simply correcting the observed logarithmic creep rate R, and the results given are always appropriately corrected.

Figures 6 and 7 show examples of the dependence of the creep rate on magnetic history for two of the alloys

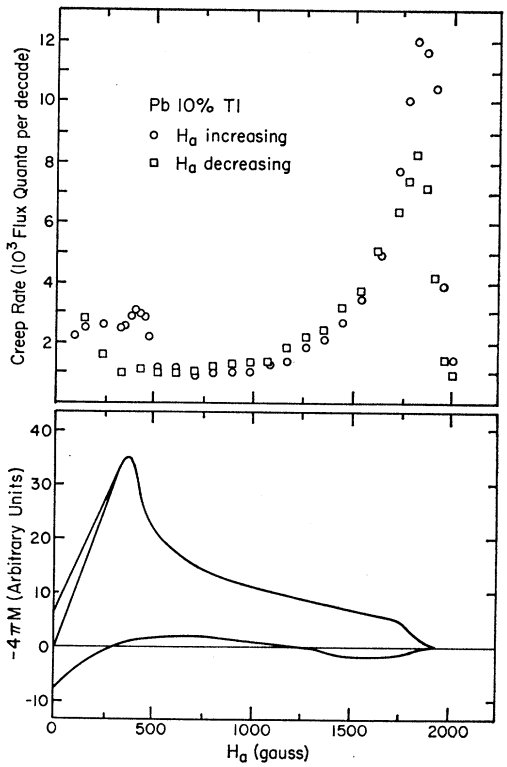

FIG. 6. Creep rate for Pb-10%Tl in the critical state. The magnetization curve is shown for reference.

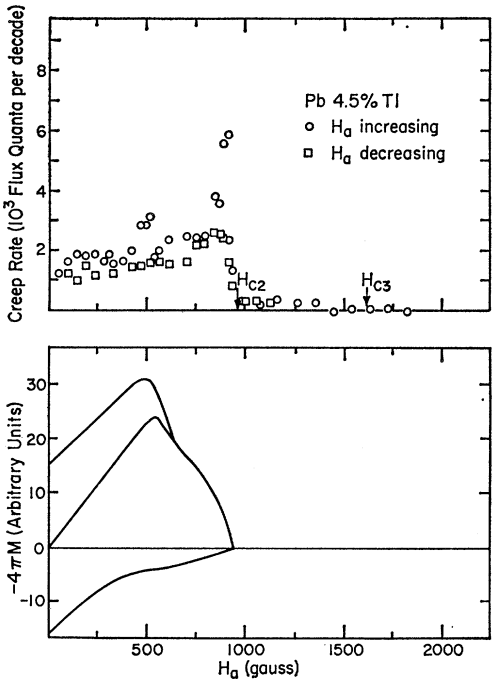

FIG. 7. Creep rate for Pb-4.5%Tl in the critical state and above H_{c2}. The magnetization curve is shown for reference.

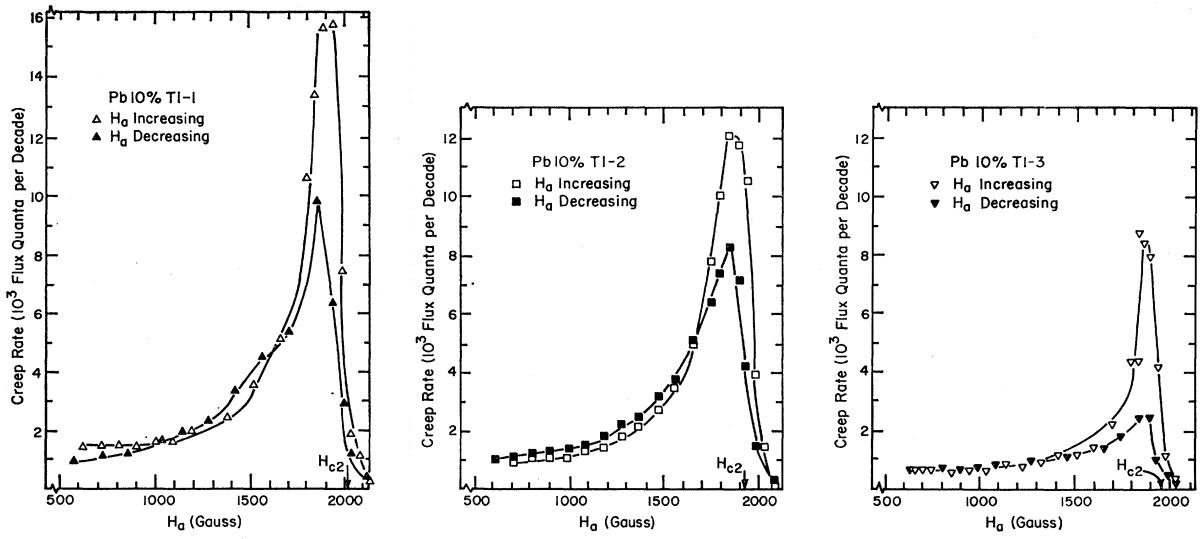

FIG. 8. (a) High-field creep rate for Pb–10%Tl-1; (b) high-field creep rate for Pb–10%Tl-2; (c) high-field creep rate for Pb–10%Tl-3.

studied. The magnetization curve for each alloy is also shown for reference. The cold-worked Pb-10%Tl specimen (Fig. 6) shows most clearly the characteristic features found in all the specimens studied. The important features are a modest increase in the creep rate for increasing fields in the region above H_{c1} and a broad rise at high fields as H approaches H_{c2}. Also, at high fields the creep rate for increasing fields $R\uparrow$ was always found to be substantially greater than the rate for decreasing fields $R\downarrow$ while at intermediate fields they were found to be comparable.

A lower-κ specimen Pb 4.5%Tl (Fig. 7) is seen to show essentially the same behavior except that the field scale is compressed due to the lower value of H_{c2}. The lower κ specimens also showed the additional feature of logarithmic decays between H_{c2} and H_{c3}. The observation of logarithmic decays in this surface-superconductivity region provides strong evidence that the nonequilibrium surface currents that exist in this region also decay via a thermally activated process. However, cold-worked lead and lead alloys are known[16] to exhibit anomalous superconductivity above H_{c2} which is not attributable to conventional surface superconductivity, and some connection between the observed decays and this effect is possible. Creep in this region should be interesting to study in the future.

The dependence of the creep rate on magnetic history was studied systematically for PbTl alloys with 0.6, 4.5, and 10%Tl and for PbIn alloys with 2 and 8% In, and in each case the results were in qualitative agreement with the examples shown above. In some of these alloys flux creep was also briefly investigated in the nominally diamagnetic region of the initial magnetization curve, and as expected, no flux creep, which would be indicative of flux penetration, could be detected below H_{c1}. After flux penetration the creep rate was found to rise rapidly as the applied field was increased until it smoothly joined the curve for the cycled magnetic state.

The effect of cold working on the creep rate is illustrated in Fig. 8, where the field dependence of the creep rate for one severely cold-worked and two partially annealed Pb-10%Tl samples is compared. The cold working was introduced by extruding the samples at liquid-nitrogen temperature with about 90% reduction of area, and the annealing was achieved by warming some of the extruded samples to room temperature for from 30 sec to several minutes. For reference, the current densities J_c for these specimens are shown in Fig. 9.

With these data it is possible to exhibit the dependence of the logarithmic creep rate on the magnitude

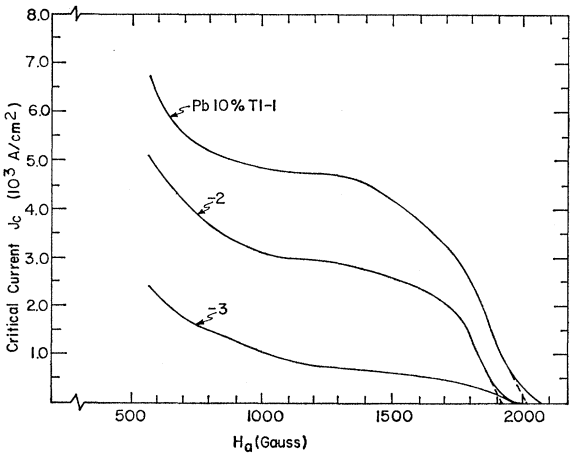

FIG. 9. Critical current for Pb–10%Tl-1, -2, and -3.

[16] W. F. Druyvesteyn and D. J. van Ooijen, Phys. Letters 4, 17 (1963); W. F. Druyvesteyn, Phillips Res. Rept. Suppl. 2 (1966).

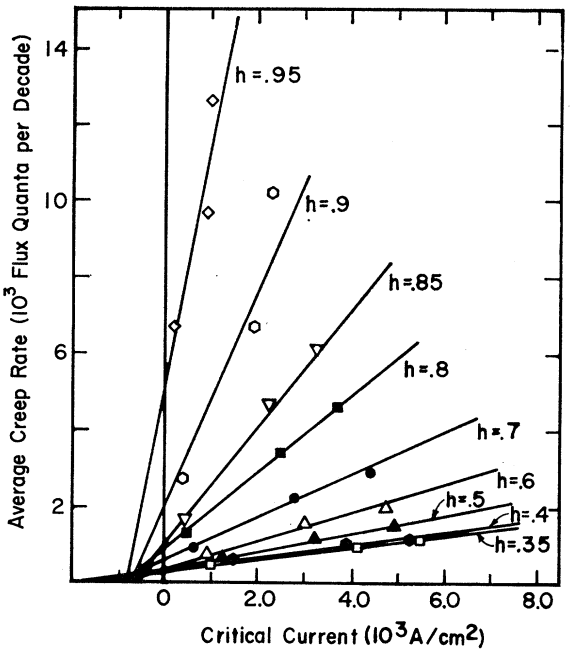

FIG. 10. Dependence of the average logarithmic creep rate R_{av} on critical current density. Three levels of deformation are compared by plotting the creep rate versus the observed critical currents for various reduced fields.

of the critical current density J_c as shown in Fig. 10, where R_{av} is plotted versus current density J_c for various reduced fields. R_{av} is the average of $R\uparrow$ and $R\downarrow$ as discussed in Sec. II. The data are plotted at constant reduced field H/H_{c2}, since field-dependent quantities affecting the creep rate are likely to be universal functions of this reduced field. However, broadening of the magnetic transition at H_{c2} made a unique determination of H_{c2} ambiguous, and the upper critical field determined from the extrapolation of J_c to zero was arbitrarily used to choose H_{c2} for normalization. Since R and J_c are rapidly varying functions of field only very near H_{c2}, only the curves for $h=0.90$ and 0.95 in Fig. 10 are noticeably sensitive to the uncertainty of H_{c2}.

Figure 10 shows that R_{av} increases linearly with the critical current J_c as expected. However, it does not quite extrapolate to zero at $J_c=0$. We suppose that this occurs because, in these experiments, the value of J_c is varied by the amount of annealing, which may also affect R through parameters other than J_c that may also be sensitive to the dislocation density and arrangement as altered by cold working and annealing. In particular, we suspect that U_0 and VX may be directly altered. Recall that we expect $R_{av} \propto J_c/U_0$, so the behavior shown in Fig. 10 may depend on an additional effect of annealing on U_0, which is not explicitly accounted for in this plot. We will return to this question later.

Specimen size, that is the wire radius ρ, appears cubed in Eqs. (2.16). The dependence of the logarithmic creep rate R on ρ can be deduced from our measurements of R on specimens with three different radii. To minimize the effects of variations of specimen preparation in this comparison, all of these specimens were cold-worked and annealed similarly. Remaining effects due to small differences in J_c were eliminated by considering the ratio R_{av}/J_c rather than R_{av} itself. This normalization procedure is justified both by theory and by the experimental observation that R_{av} is nearly proportional to J_c. The current densities in the samples used to plot Fig. 11 provide a measure of the amount of deformation. They agreed within 25%, so the normalization procedure actually introduced only a small correction. Using the dependence of U_0 on cold working, which is deduced later in this paper, we found that the remaining uncertainties are negligible in an analysis based on Eq. (2.16).

The results are shown in Fig. 11 as a logarithmic plot of R_{av}/J_c versus ρ. They substantiate an ρ^3 dependence within the experimental uncertainty and clearly eliminate the alternative ρ^2 dependence expected for a surface creep barrier. From this ρ^3 dependence we conclude that the creep process is really a bulk phenomenon rather than surface-limited. The behavior above H_{c2} was not studied systematically enough to determine whether the expected ρ^2 behavior would appear there.

Some preliminary experiments on the temperature dependence of the creep rate were also made on the Pb-10%Tl alloys. The results are incomplete because the available experimental arrangement provided

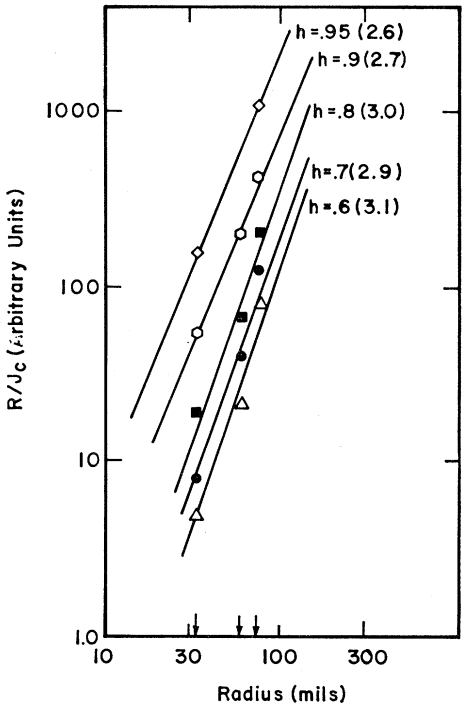

FIG. 11. Size dependence of the creep rate. The slope of each line is indicated in parentheses.

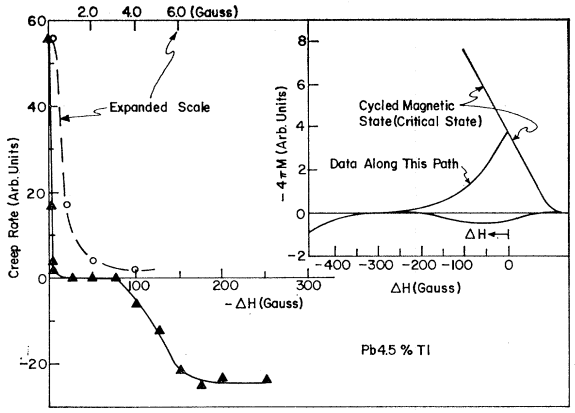

FIG. 12. Effect of field reversal for Pb-4.5%Tl. This figure illustrates the reduction in creep rate for departures from the critical state. The initial decrease is shown on an expanded scale for clarity and the insert illustrates the magnetic history for which the data were taken.

sufficiently precise temperature control only for temperatures below the lambda point of liquid helium, where H_{c2} of the Pb-10%Tl alloys unfortunately exceeded the capacity of the magnet. Therefore, it was not possible to get a complete set of high-field data to compare with the 4.2°K data. However, the incomplete results indicate that at 2.1°K the creep rate for corresponding reduced fields is approximately the same as at 4.2°K, although J_c was doubled by reducing the temperature to 2.1°K.

In addition to the preceding study of flux creep in the critical state, the effects of field and temperature departures from the critical state on the decay of the magnetization were also briefly investigated. Such excursions dramatically affect the rate of decay. For example, if field departures from the cycled (critical-state) magnetization curve were made by introducing small field reversals after an otherwise monotonic change, the decays were still logarithmic in time, but the logarithmic creep rate R was vastly reduced. For sufficiently large field reversals, R changed sign and eventually approached the rate associated with the cycled magnetization curve for field sweeps of the opposite sense. Figure 12 shows the decrease in R as a function of ΔH for a Pb-4.5%Tl specimen. For the particular case shown, the field reversals were made from a field of 800 G, and the path of the magnetization curve along which the data were taken is shown in the insert. All specimens in which field reversals were studied showed qualitatively similar behavior.

The magnitude of the reduction in R following a particular amplitude of field reversal depended on the time delay between the initial, forward field change and the field reversal. It was found that longer delays produced a greater reduction in R for a given ΔH. For the data shown in Fig. 12, the field reversals were made after a constant delay of a fraction of a second.

Temperature departures from the critical state also dramatically affected the decays. If the temperature of the specimen was lowered after a field change had been made, the decays were still logarithmic but the creep rate was observed to decrease exponentially with the magnitude of the temperature change. The results are illustrated for a typical case in Fig. 13. In these measurements the temperature changes were completed in about 5 sec, and the subsequent creep was observed to be logarithmic for as long as 1000 sec. Following temperature increases, the creep rate returned very quickly to essentially its original value. This behavior reflects the fact that after a temperature increase the flux distribution could rapidly adjust itself to the appropriate critical state, and consequently the transient response to the actual departure from the critical state was too fast to be measured in the present experiments.

As a byproduct of some of our measurements of the rate of flux creep, it was also possible to observe directly some of the details of the manner in which flux enters and leaves the specimen by analyzing the step structure seen in the magnetometer output signal (Fig. 4). This step structure indicates that much of the total flux change is made by increments of fluxoids

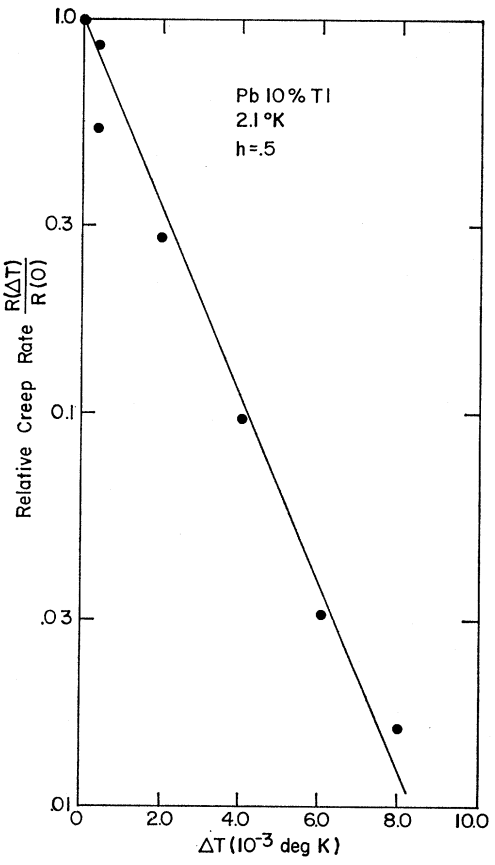

FIG. 13. Reduction in the creep rate for temperature departures from the critical state.

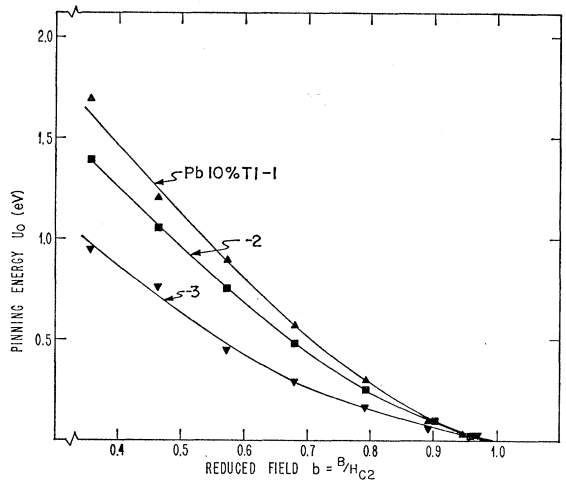

FIG. 14. Pinning energy for Pb-10%Tl. This figure illustrates the field dependence of the pinning energy for various levels of cold working.

entering (or leaving) the specimen in discrete events. This discrete character of the flux changes in the flux creep regime has been observed before by Kim, Hempstead, and Strnad[8] with conventional pickup coils.

The size of the steps shown on the recording does not represent the actual amount of flux which entered or left the specimen in an individual event, but rather the fraction of that actual amount which coupled with the primary of the superconducting flux transformer. This coupling depends on the relative magnitudes of the length along the sample over which the event took place, the radius and length of the primary, and on the location of the event along the sample. A preliminary study of the distribution of step sizes and a crude analysis of the coupling effects indicates that the increments of flux entering or leaving the material were at least as large as those seen in Fig. 4 but could have been much larger. This analysis also provides an estimate of the volume of flux contained in a distinguishable event and indicates that a typical event would have a volume of $\sim 10^{-10}$ cm^3. However, roughly 10–20% of the flux crossed the specimen surface in events so small as to be unobserved as discrete events in our experiments.[17]

V. DISCUSSION OF THE CHARACTERISTICS OF FLUX CREEP

The discussion of our experimental results proceeds in three parts. First, we consider the results pertaining to the critical state, where our theoretical analysis of creep applies, so that a detailed comparison with theory is possible. Second, we discuss the dramatic effects of departures from the critical state, where only a qualitative comparison with theory is possible, and finally in a separate section we compare our results with current models of fluxoid pinning.

A. Flux Creep in the Critical State

In the "high-field" region $H_{c1} \ll H \lesssim H_{c2}$ of the critical state the results are clearest. Here, the theoretical predictions can be expressed in a concise form [Eqs. (2.16)] and the flux-creep process is well defined and amenable to a systematic study. This regime will occupy most of our attention, but first the behavior at low fields is considered.

At low magnetic fields, erratic and irreproducible decays precluded straightforward study or analysis. However, two qualitative conclusions about the low-field behavior are possible. First, it seems quite clear that the erratic low-field behavior is related to the tendency of hard superconductors to display instabilities (flux jumps) and complicated surface effects at low fields. Second, the region of enhanced creep rate observed just above H_{c1} for increasing but not decreasing fields seems to be associated with the presence of the penetration front, where $B \to 0$, that passes through the specimen in this field region.

We now proceed with our discussion of the high-field results. For illustration, we compare the results obtained on the Pb-10%Tl alloy with the theoretical foundation for Eqs. (2.16).

The ρ^3 size dependence predicted by Eq. (2.16) seems to be satisfactorily confirmed by these experiments. The quantitative agreement for the power of ρ shown in Fig. 11 is precise except at the highest reduced fields. Most important is the conclusion that, although the data may be subject to small errors due to inexact normalization of all variations of cold working, the data are certainly good enough to rule out the ρ^2 dependence that would be expected if a surface barrier controlled the rate of flux creep.

The absence of surface effects in the creep rate below H_{c2} is significant, since a sizeable fraction of the hysteresis present in low-κ alloys is frequently attributed to surface effects. This result implies that in the critical state, where any surface current is also at its critical level, the flux creep in the bulk of the sample away from (or towards) the surface is fast enough to overwhelm the surface barrier. This interpretation is supported by the theoretical estimates made in Appendix B. However, we will suggest later that surface barriers appear to have a dramatic effect on the creep rate if field departures are made from the critical state.

According to our theoretical results, the average logarithmic creep rate should be directly proportional to J_c, the current density at the surface of the specimen. However, as we have already pointed out, in these

[17] E. Rocklin and G. I. Heiden have described more detailed measurements of the power spectrum of flux jumps during slow sweeps of magnetic field on Pb-In-alloy cylinders. Their results appear to be similar to ours except that in the creep regime we may have had a larger fraction of very small flux jumps not resolvable in their experiments. See in *Proceedings of the Conference on Fluctuations in Superconductors* (Stanford Research Institute, 1968) p. 227, and G. I. Heiden and E. Rocklin, Phys. Rev. Letters **21**, 691 (1968).

experiments J_c is determined by the amount of annealing and therefore any discussion of the observed behavior of R_{av} on J_c shown in Fig. 10 must include the effects of annealing on all the material-sensitive parameters of the theory. Equation (2.16) indicates that we should expect $R_{av} \propto (4\pi/c)J_c/U_0 = 4\pi/\gamma BVX$. To clarify what behavior might be expected from such a dependence, we consider two limiting cases. First, consider the case where the amount of annealing affects only the number of individual pinning barriers but not their individual pinning strengths (e.g., independent single-dislocation–single-fluxoid pinning). In such a case U_0 would be a constant for a given reduced field independent of the amount of annealing and R_{av} would be directly proportional to J_c. At the other extreme, in the model where annealing only affects the strength of the pinning barriers but not their density, U_0 would increase with the amount of cold working but VX would remain constant and R_{av} would be constant for a fixed field independent of J_c. Of course, if both U_0 and VX depend on the amount of cold working, the situation is more complicated, and *a priori* no exact prediction can be made. In Fig. 10, the creep rate is seen to scale with J_c but does not quite extrapolate to zero as $J_c \rightarrow 0$. This behavior is intermediate between the two extreme cases, but closest to the constant-U_0 case. We conclude that both U_0 and VX must be slightly dependent on the amount of annealing.

Thus far, we have found that the experimental results are in complete accord with the behavior expected on the basis of the theory. In particular, the measured decays have shown the predicted time and size dependence and have shown behavior consistent with the predicted dependence on current density. With these assurances that the theoretical forms correctly describe the experimental results, we can use the theory to calculate the material sensitive parameters from the experimental data.

Using Eq. (2.16) and the measured creep rates and current densities, we can calculate the field dependence of U_0 and VX at 4.2°K and estimated their changes as temperature is decreased. Figures 14 and 15 show the dependence of U_0 and VX on magnetic induction. The appropriate value of magnetic induction for a given applied field was determined directly from the hysteretic magnetization curves using the procedure of Fietz *et al.*[15] Analysis of these curves shows that both U_0 and VX decrease with increasing field roughly as $(H_{c2}-B)^{3/2}$ at least for $H > \frac{1}{2}H_{c2}$. However, VX seems to level off to a constant nonzero value as $B \rightarrow H_{c2}$ instead of extrapolating to zero. These figures also show that U_0 decreased upon annealing while VX increased. The preliminary data taken at 2.1°K indicate that $U_0(2.1°) \approx U_0(4.2°)$ and $VX(2.1°) \approx 0.6\ VX(4.2°)$. While this estimate is admittedly very crude, it does suggest that U_0 is relatively temperature-independent at these temperatures, while VX is almost certainly decreasing with temperature.

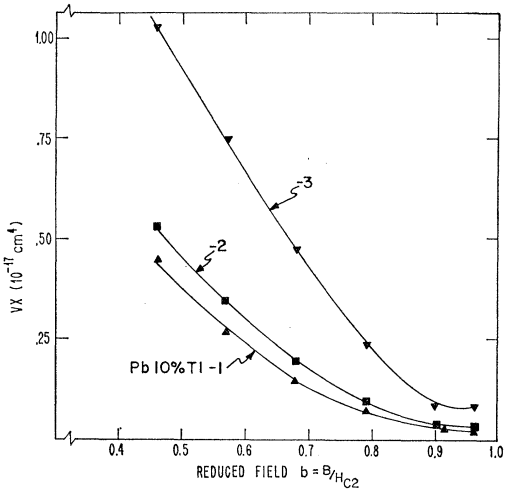

FIG. 15. Bundle-size parameter VX for Pb-10%Tl. This figure illustrates the field dependence of VX for various levels of cold working.

One of the most significant features of Fig. 15 is the fact that the decrease in VX as $H \rightarrow H_{c2}$ levels off and extrapolates to a nonzero value at H_{c2}. Equation (2.16) indicates that $VX \propto 1/R$, and the behavior of VX near H_{c2} is related to the fact that R peaks near H_{c2} rather than continuing to increase. In calculating U_0 and VX we have analyzed the data up to the peak but not beyond. By extending our analysis that far, we are implicitly neglecting any extraneous smearing of the transition at H_{c2}. Thus the exact interpretation of the data near H_{c2} and the calculated values of U_0 and VX above $b = 0.9$ are somewhat uncertain. The experimentally determined dependence on ρ also showed some discrepancy in this field region. However, we note, that there is no sign of peculiar behavior in the curve for U_0 near H_{c2}, which suggests that our analysis is reliable at these high fields. As we shall show later, a nonzero value of VX near H_{c2} is not unexpected and is physically quite appealing. However, the data presented here do not demonstrate it unambiguously.

As we shall see later in comparing our results with specific pinning mechanisms, the width of the energy barrier is expected to be $\sim 10^{-15}$ cm for all of the pinning mechanisms which appear to be relevant in these materials. Using this as an estimate for X, we find that the activation volume V is about 10^{-12} cm^3 at intermediate fields dropping at least to $\sim 10^{-14}$ cm^3 at H_{c2}. Comparing this estimate for V with our previous estimate for the volumes of flux (10^{-10} cm^3) which typically enter the specimen in one discrete step, we see that the volume of flux which acts on a given pinning barrier is much smaller than the largest total volume of flux which eventually is depinned in a particular thermally activated event. This suggests that some thermally activated events actually trigger a depinning instability or alternatively that the surface can affect the size of the increments of flux which pass through the surface,

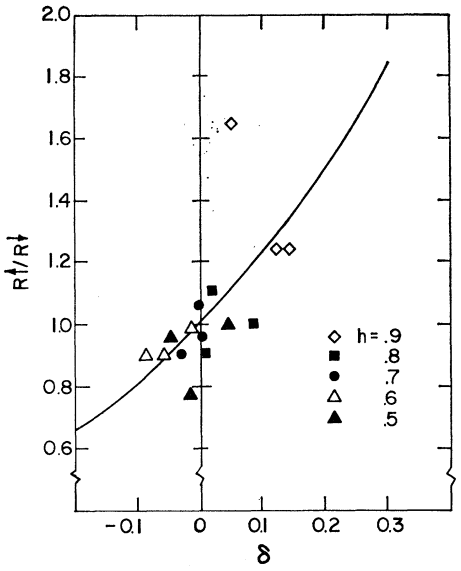

FIG. 16. Dependence of creep rate on expansion parameter δ. Solid line indicates the expected ratio $(1+\delta)/(1-\delta)$ of creep rates for increasing and decreasing fields, and points indicate the observed behavior for Pb–10%Tl-1, -2, and -3.

even though it does not control the net rate at which flux passes.

It was generally observed in these experiments that $R\uparrow \neq R\downarrow$, and we have used R_{av} in discussing the results in order to avoid this complication. To show that the use of R_{av} is justified, it is necessary to show that δ in Eqs. (2.16) is less than unity. However, it is possible to do more than this and actually to check the dependence of R on δ. This is shown in Fig. 16, where the experimentally measured ratio $R\uparrow/R\downarrow$ for the Pb-10%Tl alloy is plotted versus δ calculated from the measured current densities J_c and the calculated values of U_0, using Eq. (2.16b). The solid line is a plot of $(1+\delta)/(1-\delta)$ and indicates the theoretical prediction. Although the data points show considerable scatter, the over-all agreement is satisfactory. It provides some additional verification of the theoretical predictions and justifies the use of R_{av} in the data analysis above.

In addition to the extraction of U_0 and VX from the experimental data, it is also possible to estimate the activation energy U and the hop rate ν. From the relation $R/t=2\pi\rho D$ and the definition of D, we find that $U=kT\ln(2\pi t\rho Bw\nu_0/R)$. Assuming that ν_0 might be as large as 10^{12} sec^{-1} (a typical crystal-lattice frequency) or as small as 10^2 sec^{-1} (a fluxoid lattice frequency) and $w\approx 10^{-5}$ cm, and using the typical quantities $t=100$ sec, $B=1000$ G, and $R=6000$ flux quanta per decade for our experiments, we find U could be as large as 34 kT ($\approx$0.014 eV) or as small as $7kT$($\approx$0.003 eV). Of course, U will increase very slowly in time as the field gradients decay, but the values calculated here are appropriate for normal laboratory time scales. With the extremes of ν_0 assumed above, the actual hop rate at each pinning barrier is somewhere between 10^{-3} and 10^{-1} sec^{-1}.

With this estimate of U it is possible to compare the three energies involved in the thermal activation process. This comparison indicates that $kT\ll U\ll U_0$ except very near H_{c2}, where U_0 may become comparable to U, and justifies our neglect of higher-order terms in the solution of the flux-creep equation.

One possible source of error in our analysis of the creep results arises from an uncertainty in J_c due to surface currents. The critical currents were determined from the hysteretic magnetization curves using the procedure of Fietz *et al.*[15] and in this procedure any hysteresis in the magnetization due to nonequilibrium surface currents is considered as arising from bulk currents. Thus the values of current shown in Fig. 9 and used in the analysis of the high-field results are upper limits to the true bulk currents.

The current state of theory and experiment regarding the magnitude of these surface currents is still quite unsettled so it is difficult to reliably estimate them for a particular case. However, using the data of Hart and Swartz[18] for the surface currents in films of Pb–10%Tl below H_{c2}, we estimate that surface currents could produce hysteresis comparable to that observed for Pb–10%Tl-3. On this basis, the errors in J_c for Pb–10%Tl-3 could be considerable, but not more than 20% and 10% for Pb–10%Tl-2 and -1, respectively.

These possible errors in J_c would have the following effects on the results discussed so far. The log-log plot of R_{av}/J_c versus ρ (Fig. 11) would not be seriously affected since the data were taken for large J_c where the error in J_c is small and therefore does not modify our conclusion about surface barriers. The R_{av} versus J_c curve (Fig. 10) would be flattened even more, since the data taken on Pb–10%Tl-3 would be moved to the left, and consequently the calculated values of U_0 for Pb–10%Tl-3 might be somewhat smaller than indicated. There would be no error in VX, since it can be determined independently of J_c. At worst these errors seriously affect only one specimen, and considering the similar behavior observed for the three specimens, we feel confident that these surface currents are not affecting the results in any qualitative way.

B. Departures from the Critical State

Field and temperature departures from the critical state (Figs. 12 and 13) were observed to reduce dramatically the rate of flux creep into (or out of) the specimen. In both cases, the rapid attenuation in creep rate can be accounted for by at least part of the material transferring to a subcritical state.

The case of temperature departures can be explained more completely. Since the critical current density J_c usually increases for decreasing temperature, a tempera-

[18] H. R. Hart and P. S. Swartz, Phys. Rev. **156**, 403 (1967).

ture decrease ΔT made after establishing the critical state places the entire specimen in a state in which the initial current density $J_c(T)$ is less than that current appropriate in the critical state at the lower temperature $J_c(T-\Delta T)$. In this subcritical state, the activation energy required for fluxoid motion is higher, and therefore the rate of flux creep should be reduced. More explicitly, from the relation $\partial\phi/\partial t=-2\pi\rho D(\rho,t)$ and the definition of D, we see that immediately after a temperature decrease ΔT

$$\left.\frac{\partial\phi(t)}{\partial t}\right|_{T-\Delta T}=e^{[\partial(U/kT)/\partial T]_\rho \Delta T}\left.\frac{\partial\phi(t)}{\partial t}\right|_{T},$$

where $[\partial(U/kT)/\partial T]_\rho$ is evaluated at the surface and the derivative is taken at constant $|\nabla B|$. This equation shows that immediately after the temperature decrease, the flux creep should exhibit a logarithmic decay with a rate attenuated exponentially in ΔT. This completely accounts for the observed behavior, and from the data in Fig. 13 we find $\partial(U/kT)/\partial T=2000\ \mathrm{K}^{-1}$, a result which is consistent with the preliminary data on the temperature dependence of U_0 and VX.

The behavior after a field departure is more complicated. When a small field reversal is made from the critical state, the net effect is to decrease the surface current to a subcritical level, thereby creating an enhanced surface barrier. The presence of a significant surface barrier clearly explains the rapid attenuation of the flux creep through the surface for small ΔH. However, the creation of a surface barrier does not immediately affect the rate of creep in the interior, and the persistence, even if only momentarily, of unattenuated flux creep in the interior tends to compensate the effect of a field reversal by building up the surface current back toward its critical value. This compensation effect makes a theoretical description of the behavior following a field reversal quite complicated, and we have not undertaken a detailed calculation. An additional complication arises, since the degree of compensation depends on the rate of flux flow away (or towards) the surface at the time of the field reversal and therefore the behavior becomes a function of the time the field reversal was made. Just such a time dependence was observed experimentally.

It is perhaps worth noting that these dramatic reductions in the creep rate produced by departures from the critical state are of practical importance in situations where it is desirable to suppress flux creep.

VI. FLUX CREEP AND PINNING MODELS

One of the ultimate purposes of our flux-creep measurements was to learn something about the basic interaction mechanisms leading to magnetic hysteresis in superconductors. We sought to determine the physical nature of the crystalline defects which provide the activation barriers, to test the validity of specific pinning models, and if valid, to determine their free parameters. For this purpose we have to outline first the relations between pinning models and the parameters of the creep theory. We characterize the elementary interaction between a single defect and a fluxoid by an energy ϵ, a geometrical width d of the defect (for instance the diameter of a small precipitate), and the volume concentration C of defects. The question is then ,what information on the parameters ϵ, d, and C can be gained from a knowledge of the quantities U_p and VX_p which are characteristic of the activation barriers and can be obtained from flux-creep measurements using only Anderson's thermal-activation theory independently of any specific models of pinning.

Obviously, the defect width is just the barrier width X_p if d is larger than the coherence length ξ but smaller than the lattice constant of the fluxoid lattice, which is roughly $(\phi_0/B)^{1/2}$. On the other hand, if d is larger than $(\phi_0/B)^{1/2}$, $X_p\simeq(\phi_0/B)^{1/2}$ because of the periodicity of the fluxoid lattice, and if d is smaller than the coherence length ξ, $X_p\approx\xi$ because the range of the elementary interaction between fluxoid and defect X_p cannot be smaller than the coherence length ξ, which is a lower limit to the range of any interaction. Therefore, we expect $X_p\approx\xi$ if $d<\xi$, $X_p\approx d$ if $\xi<d<(\phi_0/B)^{1/2}$, and $X_p\approx(\phi_0/B)^{1/2}$ if $d>(\phi_0/B)^{1/2}$.

Thus a connection between X_p and d can only be made for a rather limited range of values of d. On the other hand, this has the advantage that the value of V alone can always be obtained within certain limits although from the experiments only the product VX_p can be obtained where we take $X_p\approx X$.

The "activation volume" V defines the region of transfer of the volume force $-\gamma(B/4\pi)\nabla B$ to an activation barrier so that the force $V\gamma(B/4\pi)\nabla B$ is acting on it during an activation event. For a low defect density C we expect therefore that $V\approx 1/C$ and that the barrier height U_p is equal to the interaction energy ϵ of a single defect. There is, however, a lower limit V_0 below which the value of V cannot go when C is increased. The reason is that fluxoids are strongly coupled to each other and form a rather rigid lattice in which they can be activated only in a collective way, involving many fluxoids in a single activation process. If the volume of flux involved in such a collective process is larger than $1/C$, the simple picture in which U_p and V are directly related to ϵ and $1/C$ is no longer applicable. Anderson's concept of flux bundles[3] is a qualitative expression of this fact.

To be a little more specific about this problem, we propose the following model, which is more detailed though also only qualitative in its results: During an activation process, the volume V undergoes a displacement versus the surrounding fluxoid lattice. The displacement at the center of the volume is about equal to the observed activation length X. The displacement yields the energy $VX\gamma(B/4\pi)\nabla B$ coming from the

general volume force on all fluxoids but at the same time a distortion energy $U_1 \approx (G/2)V^{1/3}X^2$ is required. Here, G is a combination of the elastic moduli of the fluxoid lattice,[19–21] its exact form depending on the shape of the activation volume and the distribution of the displacement between the center of V and the outside of V, where the displacement goes to zero. The net energy which is available to support the thermal activation is then only $VX(B/4\pi)\nabla B - U_1$ instead of $VX\gamma(B/4\pi)\nabla B$. If the shape of the activation volume is taken ellipsoidal, the displacement being X at the center and falling off to the outside like a Gaussian, and if the axes of the ellipsoid are chosen to make U_1 a minimum for a given volume, a simple calculation shows that $G \approx (C_{11}C_{44}C_{66})^{1/3}$, where C_{11}, C_{44}, and C_{66} are the elastic moduli of the fluxoid lattice in Voigt's notation. Thus, in order to have a net energy gain at all, it is necessary to have $VX\gamma B\nabla B/4\pi - U_1 > 0$ and therefore V must be larger than $V_0 = (GX/2\gamma(B/4\pi)|\nabla B|)^{3/2} \propto (C_{11}C_{44}C_{66})^{1/2}$. If V_0 happens to be larger than $1/C$, there will be no direct relation between the activation volume and the defect concentration. Furthermore, the barrier height U_p as well as activation energy U_0 will be given by the net effect of all the defects contained in V rather than by the interaction energy ϵ of a single defect.

A quantitative theory would have to take into account the dependence of the net barrier U_p on the magnitude of V, combine it with the V dependence of the energy gain $VX\gamma B\nabla B/4\pi - U_1(V)$, and choose the activation volume that yields the maximum activation rate. Such a theory is not available at present. Qualitatively, the model suggests that the elastic properties of the fluxoid lattice, in particular their dependence on the magnetic field, will be reflected in the measured value of the activation volume. A recent calculation[21] shows that the shear modulus C_{66} of the fluxoid lattice drops quadratically to zero when the applied field approaches the upper critical field H_{c2}. Therefore, a strong decrease of the activation volume with increasing field is expected. Of course, since the cross section of our ellipsoidal model volume cannot be smaller than one lattice cell of the fluxoid lattice, we expect V to go to a small constant rather than zero at H_{c2}.

After these preliminary remarks we can now proceed to a comparison of our experimental results with specific pinning models: From the specimen preparation it is obvious that the pinning is provided by dislocations so we try to explain the creep data on the basis of an interaction between dislocations and fluxoids. Most striking in this connection is the observation that the measured energy U_0, which is closely related to the energy barrier U_p, is of the order 1 eV. In contrast the first- and second-order calculations of the interaction energy ϵ_0 between a single fluxoid and a single dislocation[22,23] yield only a value of the order 10^{-2} eV for ϵ_0 in Pb-Tl alloys. There might be unknown interaction mechanisms that have not been discussed so far, but an interaction energy ϵ_0 of the order 1 eV seems to be clearly out of the question. We therefore conclude that in one activation process many single dislocation obstacles (at least of the order 10^2) are overcome simultaneously. Two models,[6] based on our discussion at the beginning of this paragraph, can be proposed to account for this fact:

(1) The first model is based on the assumption that the points where a dislocation and a fluxoid are in contact are distributed at random. To estimate the volume density of these points, we assume a dislocation density N of a few times 10^{11} cm^{-2}, which as a rule of thumb is the density after severe plastic deformation, regardless of the material and of other deformation parameters. Since the geometrical width of a dislocation is supposedly about equal to the Burgers vector, we have here the case mentioned before that the width of the defect is much smaller than the coherence length ξ, so that the width of the energy barrier would be ξ. This is confirmed by the first- and second-order elasticity calculations according to which the range of the interaction is indeed the coherence length. We thus assume $X_p \approx \xi$. The cross section for an intersection between a dislocation and a fluxoid is X_p times the fluxoid length, and thus the number of contact points inside the activation volume V is $n_c \approx VX_p(B/\phi_0)N$. From the measured values of VX of the annealed specimens (ignoring the small difference between X and X_p), we obtain values of n_c between 10^4 at $B = \frac{1}{2}H_{c2}$ and 10^3 at $B = H_{c2}$. (Notice that only the measurable quantity VX enters the expression for n_c so that the assumption $X_p \approx \xi$ is not really necessary for estimating n_c.) However, the net interaction, which gives us U_p and U_0, is not simply n_c times the elementary interaction energy ϵ_0 because with a random array of dislocations most of the elementary interactions contribute only to a flat background energy and only statistical fluctuations in their number and position give rise to a net barrier. Therefore, a relation $U_p \approx n_c^{1/2}\epsilon_0$ rather than $U_p \approx n_c\epsilon_0$ is likely to apply. With $\epsilon_0 \approx 0.01$ eV, $n_c^{1/2}\epsilon_0$ is just of the order of 1 eV. Thus our model provides a reasonable explanation of the measured pinning energy. In view of the restricted range of X pointed out earlier, this model requires that VX drop to a small *nonzero* value as the field B goes to H_{c2}, as is also observed experimentally.

(2) It is known that at high levels of plastic deformation the dislocations are not distributed completely at random, but are clustered in a cellular structure with cell walls of very high dislocation density and a lower

[19] A. L. Fetter, P. C. Hohenberg, and P. Pincus, Phys. Rev. **147**, 140 (1966).
[20] R. Labusch, Phys. Status Solidi **19**, 715 (1967).
[21] R. Labusch, Phys. Status Solidi (to be published).
[22] E. F. Kramer and C. L. Bauer, Phil. Mag. **15**, 1189 (1967).
[23] W. W. Webb, Phys. Rev. Letters **11**, 191 (1963).

dislocation density between the walls. The dimensions of the cell structure are typically of the order 1 μ. There are two different mechanisms that can produce a difference between the self-energies of a fluxoid inside and outside a cell wall and thus might be responsible for pinning by cell walls.

(a) From the second-order elasticity interaction an energy difference $\Delta E \approx \xi \Delta N \epsilon_0$ per unit length of fluxoid is obtained, where ΔN is the difference between the dislocation densities inside and outside the wall and ϵ_0 is the interaction energy with a single dislocation. With $\xi \approx 4\times10^{-6}$, $\Delta N \approx 10^{11}$ cm^{-2}, and $\epsilon_0 = 10^{-2}$ eV, we obtain $\Delta E = 4\times10^{3}$ eV/cm.

(b) There is a difference of the mean free path inside and outside the cell wall and consequently a difference $\Delta\kappa$ of the Ginsburg-Landau parameter κ and a difference of ΔE of the self-energy of a fluxoid. Willis, Schenk, and Shaw[24] have estimated this energy difference using κ differences inferred from the observed smearing of the transition at H_{c2}. Their experiments were, like ours, done on Pb-Tl alloys, however, with a somewhat higher Tl concentration than used here. They find an interaction energy $\Delta E \approx 10^{+4}$ eV/cm per unit length of fluxoid.

Considering now the interaction with a cell wall instead of a single dislocation, we obtain an interaction energy $\epsilon = \Delta E l_c$, where l_c is the length over which a fluxoid is in contact with a cell wall. Assuming that l_c is roughly equal to or somewhat smaller than the cell diameter $d \approx 10^{-4}$ cm, we find that both the second-order elasticity interaction and the interaction via a modulation of the mean free path can be considered as possible explanations for an interaction energy of the order 1 eV. In this model the volume concentration of obstacles is low and one compound obstacle alone already provides the full energy barrier obtained from the creep experiments. Therefore, the activation volume is expected to be $V \approx 1/C$, where the obstacle density C is given by $C \approx (B/\phi_0)^{1/2}\, 1/d^2$. Since the dimensions of the cells are larger than the lattice constant of the fluxoid lattice, we assume $X_p \approx (\phi_0/B)^{1/2}$. Thus, $VX \approx d^2(\phi_0/B)$. Inserting $d \approx 10^{-4}$ cm and the typical value 1000 G for B, we obtain $VX = 2\times10^{-18}$ cm^4, which is also comparable with the experimental value. The two models presented here in (1) and (2) are not mutually exclusive since there can be pinning by random dislocation in the interior of cell walls *and* extra pinning at the edges of the walls. Both models provide an explanation for the high observed value of U_0. No quantitative prediction on the behavior of VX with field can be given for model (1), but qualitatively it is in agreement with the experiment. Model (2) yields the quantitative relation $VX \sim 1/B$ which is *not* in agreement with the experiments. Proportionality to $1/B$ would only account for a ratio of 2 between the values of VX at $B = \frac{1}{2}H_{c2}$ and $B = H_{c2}$ while the observed ratio is larger than 10. Thus, the experimental evidence is in favor of our first model as describing the dominant mechanism by which flux creep is controlled, but we feel that more independent experiments should be done before drawing a definite conclusion and that alternative explanations, not discussed here, cannot now be completely ruled out. Detailed observations of the dislocation structures of the actual specimens measured is particularly necessary.

[24] J. S. Willis, J. F. Schenk, and R. W. Shaw, Appl. Phys. Letters **10**, 101 (1967).

VII. SUMMARY

These experiments have considerably enlarged our experimental knowledge of the characteristics of flux creep in hard superconductors; they are in complete accord with the predictions based on Anderson's theory of flux creep, and they have demonstrated the usefulness of flux-creep measurements in providing detailed, quantitative information about the pinning mechanisms which underlie the properties of hard superconductors.

The observed characteristics of the flux-creep process are complex in detail, and therefore the general characteristics in the materials studies and their interpretation are recapitulated here in a brief form:

(1) A logarithmic time dependence of the creep process prevails in the critical state, due to exhaustion of the excess of the driving forces over the pinning forces as creep proceeds.

(2) The logarithmic rate of change of the total flux in a cylindrical specimen initially cycled to the critical state is given approximately by

$$\left(\frac{d\phi}{d\ln t}\right)_{\rm av} \equiv R_{\rm av} \cong \tfrac{1}{3}\pi k T \rho^3 \frac{4\pi}{\gamma B}\frac{1}{VX} = \tfrac{1}{3}\pi k T \rho^3 \frac{4\pi}{c}\frac{J_c}{U_0},$$

where the averaging approximation and the symbols are defined in the discussion leading to Eqs. (2.16).

(3) For magnetic fields small enough to preserve the Meissner state, creep is undeterminably small but peaks as field penetration begins and rises again as $H \to H_{c2}$. Flux creep above H_{c2} is detectable in some cases and may indicate thermally activated decay of surface currents in the surface sheath regime.

(4) Determination of the material-sensitive parameters U_0 and VX from analysis of the flux-creep results suggests $U_0 \sim 1$ eV, $V \sim 10^{-12}$ cm^3, and $X \sim 10^{-5}$ cm at intermediate fields and as $H \to H_{c2}$, $U_0 \to 0$, and V approaches a nonzero value such as 10^{-14} cm^3.

(5) On departing from the critical state by decreasing temperature the logarithmic creep rate drops exponentially. On changing applied magnetic field back away from the critical-state curve, the creep rate drops precipitously, eventually becoming zero and finally reversing sign as field increments are increased.

(6) Flux crosses the specimen surface in increments containing from a very few fluxoids to, say, 10^3 or more.

(7) Flux-creep experiments support a simple collective pinning model of the sort advanced by Fietz and Webb[6] to account for their critical magnetization measurements.

ACKNOWLEDGMENTS

We are pleased to acknowledge the support of this work by the U. S. Atomic Energy Commission nearly from its beginning, through the Metallurgy and Materials Branch of the Division of Research, and the use of facilities provided by the Advanced Research Projects Administration at Cornell. Dr. Arnold Silver helped us to learn the technology of SQUID construction, and John Claassen helped with some of the experiments.

APPENDIX A: NONLOGARITHMIC CREEP

It has been assumed so far that our particular solution for $D(r,t)$, which we now call $D_{\log}(r,t)$, gives an appropriate description of the flux-creep phenomena. We show now that indeed any small perturbation of this solution decays rapidly in time, so that for large t only $D_{\log}(r,t)$ and the resultant "logarithmic creep" is left over.

Writing $D=D_{\log}(r,t)+d(r,t)$ and keeping only first orders of d, we obtain, from Eq. (2.8),

$$\frac{\partial d}{\partial t}=\frac{1}{t}\left[\psi_0(rd)+d\psi_0(r\psi)\right], \tag{A1}$$

where $\psi(r)$ is the position-dependent part of $D_{\log}(r,t)$ and ψ_0 is the differential operator

$$\psi_0=\frac{1}{kT}\left(\frac{\partial U}{\partial|\nabla B|}\right)_{t_1}\left[\frac{\partial}{\partial r}\frac{1}{r}\frac{\partial}{\partial r}-\left(\frac{\partial \ln|\nabla B|}{\partial r}\right)_{t_1}\frac{1}{r}\frac{\partial}{\partial r}\right].$$

Equation (A1) is separated by $d=\delta(t)\phi(r)$, and a complete set of solutions is obtained with $\delta_\alpha(t)=-1/t^\alpha$ from the eigenvalue equation

$$(\alpha-1)\phi_\alpha=\psi_0(r\phi_\alpha). \tag{A2}$$

The boundary conditions for ϕ_α are the same as for ψ. Since $\psi_0(r\psi)=1$, a solution of Eq. (A2) is $\phi_{\alpha 0}(r)=\text{const}\times\psi(r)$ with the eigenvalue $\alpha_0=2$. It is easy, though somewhat lengthy, to show that the eigenvalues of Eq. (A2) are monotonically increasing with the number of nodes of ϕ_α. Therefore, since ψ has no nodes at all, $\alpha_0=2$ is the lowest eigenvalue of Eq. (A2), and any perturbation $d(r,t)$ decays at least as rapidly as $1/t^2$, whereas $D_{\log}(r,t)$ decays like $1/t$.

APPENDIX B. REMARKS ON SURFACE-CONTROLLED CREEP

If there is a special barrier to flux penetration at the specimen surface, the magnetic field $B(\rho)$ just below the surface is not equal to B_a, the field that would be in thermodynamic equilibrium with the applied field. To calculate the effect of a surface barrier we assume again a thermally activated penetration of the barrier which is supported by a driving force due to the difference $|B(\rho)-B_a|$. The flux through the surface is then

$$D_s=D_{s0}\exp\left(-\frac{U_s(|B(\rho)-B_a|)}{kT}\right).$$

The boundary condition for the bulk creep has to be matched to this flux flow. The calculation of the creep rate is then a straightforward generalization of the bulk-creep analysis. The result is

$$R=\tfrac{1}{3}\pi kT\left[\frac{(4\pi/c)J_c}{U_0}\rho^3+3\frac{(4\pi/c)J_{cs}}{U_{0s}}\lambda_s\rho^2\right].$$

$U_{0s}=(\partial U_s/\partial|B(\rho)-B_a|)|B(\rho)-B_a|$ is defined in analogy to U_0 in the bulk and $J_{cs}=(c/4\pi)(|B(\rho)-B_a|/\lambda_s)$, in analogy to J_c in the bulk. λ_s is the thickness of the surface barrier, and is expected to be roughly equal to the London penetration depth.

We notice that the surface contribution to the creep rate is proportional to ρ^2, while the pure bulk creep has a rate proportional to ρ^3. Thus, an experimental distinction can be made by measuring the creep rate in specimens with different diameters under otherwise equal conditions.

It is reasonable to assume that U_0 and U_{0s} are of the same order of magnitude. A considerable contribution from the surface term is then expected only if J_{cs}/J_c is comparable with ρ/λ_s, which calls for extremely low critical currents in the bulk or for extremely thin specimens.